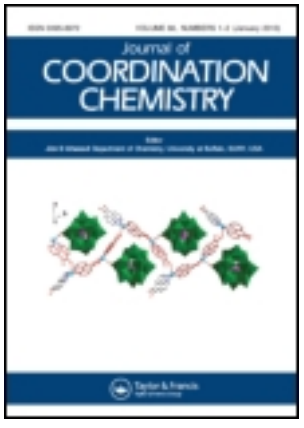

Journal of Coordination Chemistry
Publication details, including instructions for authors and subscription information:
http://www.tandfonline.com/loi/gcoo20

Metal and structure tuned in vitro antitumor activity of benzimidazole-based copper and zinc complexes

Jin'an Zhao [a], Shenshen Li [b], Dandan Zhao [b], Shufang Chen [b] & Jiyong Hu [a]

[a] Department of Chemistry and Chemical Engineering, Henan University of Urban Construction, Henan, P.R. China

[b] Department of Chemistry, Zhengzhou University, Zhengzhou, P.R. China

Accepted author version posted online: 26 Mar 2013.Published online: 29 Apr 2013.

To cite this article: Jin'an Zhao, Shenshen Li, Dandan Zhao, Shufang Chen & Jiyong Hu (2013) Metal and structure tuned in vitro antitumor activity of benzimidazole-based copper and zinc complexes, Journal of Coordination Chemistry, 66:9, 1650-1660, DOI: 10.1080/00958972.2013.789505

To link to this article: http://dx.doi.org/10.1080/00958972.2013.789505

Journal of Coordination Chemistry, 2013
Vol. 66, No. 9, 1650–1660, http://dx.doi.org/10.1080/00958972.2013.789505

Metal and structure tuned *in vitro* antitumor activity of benzimidazole-based copper and zinc complexes

JIN'AN ZHAO†*, SHENSHEN LI‡, DANDAN ZHAO‡, SHUFANG CHEN‡ and JIYONG HU†

†Department of Chemistry and Chemical Engineering, Henan University of Urban Construction, Henan, P.R. China
‡Department of Chemistry, Zhengzhou University, Zhengzhou, P.R. China

(*Received 29 November 2012; in final form 30 January 2013*)

Four new complexes, Cu_2(p-2-bmb)$_2Cl_4$ (**1**), Cu_2(p-2-bmb)$_2Br_4$ (**2**), Zn_2(p-3-bmb)$_2Cl_4$ (**3**), and $[Cu_3$(p-3-bmb)$_2Cl_4\cdot(CH_3OH)_2]_n$ (**4**), have been synthesized under solvothermal reactions based on V-shaped flexible ligands 1-((2-(pyridin-2-yl)-1H-benzoimidazol-1-yl)methyl)-1Hbenzotriazole (p-2-bmb) and 1-((2-(pyridin-3-yl)-1H-benzoimidazol-1-yl)methyl)-1Hbenzotriazole (p-3-bmb). Complexes **1–3** are binuclear, whereas **4** is an infinite chain with trimetallic units, and then these complexes are further extended into 3D supramolecular architectures by $\pi\ldots\pi$ interactions and hydrogen bonds. *In vitro* antitumor activities of these complexes on four human tumor cell lines (gastric tumor cell line, esophagus tumor cell line, liver tumor cell line, colon tumor cell line) were evaluated by MTT assay. The results exhibit that these complexes inhibit the growth of cancer cells by inducing apoptosis, and the inhibition effect shows time- and dose-effect relationship.

Keywords: V-shaped flexible ligand; Crystal structure; Antitumor activity

1. Introduction

Metal-organic coordination architectures have intriguing structures [1] and potential applications [2]. Clinical success of cisplatin for treatment of a variety of cancers has promoted extensive studies of Pt(II) complexes and non-Pt metal complexes as potential diagnostic agents and for antitumor properties [3]. Ru(III) complexes have been developed as a new family of promising metal-based anticancer drug candidate in clinical trials [4]. To gain insights into the structure–activity relationship, design and synthesis of complexes with desired structural features and biological activities remain a long-term challenge; functional group and geometry of ligands are crucial for construction of structure-specific coordination architectures.

A functional group with possibility of biomolecular interaction can greatly affect the cytotoxicity of complexes, especially for heterocyclic moieties in the bridging connector [5]. As N-heterocyclic linkers, benzimidazole and its derivatives have strong coordination abilities, and the $\pi\ldots\pi$ interactions between aromatic rings stabilize the supra-molecular system. Also, such moieties have biological activity, which can mimic the imidazole

*Corresponding author. Email: zjinan@zzu.edu.cn

function in proteins, and induce unusual coordination geometries with interesting spectral and redox properties [6].

Also, complexation of metal centers with such ligand may produce synergistic effects on the antiproliferative activities of the parent ligands, providing a dual mode of binding at the molecular target site and also exhibiting preferential selectivity inside the cells [7]. To minimize the side effects and resistance to Pt(II) complexes, non-Pt metal complexes offer alternatives, which can show various geometries and coordination numbers, feasible substitution kinetic pathways, and different pharmacological profiles. Cu(II) and Zn(II) are bioessential metal ions with less toxicity, critical for various biological systems and their complexes are preferred for cancer inhibition. Cu(II)-based compounds have selective permeability of cancer cell membranes and high site-specific binding affinities, and a number of Cu(II) complexes are active both *in vitro* and *vivo*. Certain Zn(II) complexes exhibit anticancer activities and regulate apoptosis as well [8]. [CuII(5-Cl-pap)(OAc)(H_2O)]·$2H_2O$ [9], $CuCl_2$SalPz [10], [(ETDPA)Cu(phen)](ClO_4)$_2$ [11], and [$ZnCl_2$(Ac4Npypipe)] [12], based on these metal centers, are agents with potential antitumor activity and can be selected for further stages. Four new complexes, Cu_2(p-2-bmb)$_2Cl_4$ (**1**), Cu_2(p-2-bmb)$_2Br_4$ (**2**), Zn_2(p-3-bmb)$_2Cl_4$ (**3**), and [Cu_3(p-3-bmb)$_2Cl_4$·$(CH_3OH)_2]_n$ (**4**), have been constructed by reactions of benzotriazole and benzimidazole (p-2-bmb, p-3-bmb) with Cu(II) or Zn(II) salts. The *in vitro* cytotoxicities of **1–4** to inhibit human alimentary system carcinoma cell lines: SGC7901 (gastric tumor cell line), EC109 (esophagus tumor cell line), SMMC7721 (liver tumor cell line), and HT29 (colon tumor cell line) have been evaluated by MTT assay.

2. Experimental

2.1. *Materials and general methods*

All chemicals were obtained from commercial sources and used without purification. The 2-(2-pyridyl)-benzimidazole and 2-(3-pyridyl)-benzimidazole have been prepared as previously reported [13]. Cisplatin was purchased from Jiangsu Stockhausen Pharmaceutical Co., Ltd. 1-((2-(pyridin-2-yl)-1H-benzoimidazol-1-yl)methyl)-1H-benzotriazole (p-2-bmb) and 1-((2-(pyridin-3-yl)-1H-benzoimidazol-1-yl)methyl)-1H-benzotriazole (p-3-bmb) were synthesized according to reported procedures [14]. IR spectra were recorded from 400 to 4000 cm^{-1} with KBr pellets on a BRUKER TENSOR 27 spectrophotometer. Elemental analyses for C, H, and N were carried out with a Flash EA 1112 elemental analyzer. The TG and DSC curves were performed on a TGA/SDTA instrument.

2.2. *Synthesis of Cu_2(p-2-bmb)$_2Cl_4$ (1)*

$Cu(Ac)_2$·H_2O (0.0201 g, 0.1 mM), p-2-bmb (0.0325 g, 0.1 mM), ethanol (3.0 mL), chloroform (3.0 mL), and methanol (6.0 mL) were placed in a Teflon-lined stainless steel vessel (20 mL). The mixture was heated at 80 °C for three days and then the reaction system was gradually cooled to room temperature at 5 °C h^{-1}. Green crystals of **1** were obtained. Yield: 43% (based on Cu). Elemental analysis (%) Calcd for $Cu_2C_{38}H_{28}Cl_4N_{12}$: C, 49.52%; H, 3.06%; N, 18.24%. Found: C, 49.37%; H, 3.10%; N, 17.98%. IR (KBr/pellet, cm^{-1}): 3444.71(m), 3029.26(w), 1604.56(w), 1479.25(w), 1454.33(m), 1440.43(s), 1399.13(m), 1299.64(m), 1198.34(w), 1150.35(w), 1013.04(w), 930.87(w), 752.62(s), 599.35(w).

2.3. *Synthesis of $Cu_2(p\text{-}2\text{-}bmb)_2Br_4$ (2)*

A mixture of $CuBr_2$ (0.0045 g, 0.02 mM), p-2-bmb (0.0065 g, 0.02 mM), chloroform (1 mL), and methanol (1 mL) was placed in a tightly closed glass reactor (10 mL), which was heated at 80 °C for three days and then cooled to room temperature at 5 °C h^{-1}. Brown crystals of **2** were obtained. Yield: 56% (based on Cu). Elemental analysis (%) Calcd for $C_{38}H_{28}N_{12}Br_4Cu_2$: C, 41.51%; H, 2.57%; N, 15.29%. Found: C, 41.47%; H, 2.53%; N, 15.30%. IR (KBr/pellet, cm^{-1}): 3444.24(s), 3087.03(w), 3026.94(w), 1604.25 (w), 1478.51(m), 1453.08(m), 1438.77(s), 1397.82(m), 1298.12(m), 1197.67(w), 1167.10 (w), 1104.56(w), 750.70(s), 433.56(w).

2.4. *Synthesis of $Zn_2(p\text{-}3\text{-}bmb)_2Cl_4$ (3)*

A mixture of $ZnCl_2$ (0.0027 g, 0.02 mM), p-3-bmb (0.0065 g, 0.02 mM), chloroform (1 mL), and methanol (1 mL) was placed in a tightly closed glass reactor (10 mL), which was heated at 80 °C for three days and then cooled to room temperature at 5 °C h^{-1}. White crystals of **3** were obtained. Yield: 51% (based on Zn). Elemental analysis (%) Calcd for $Zn_2C_{38}H_{28}Cl_4N_{12}$: C, 49.32%; H, 3.05%; N, 18.16%. Found: C, 49.35%; H, 3.03%; N, 18.04%. IR(KBr/pellet, cm^{-1}): 3466.53(m), 3001.08(w), 1612.31(m), 1454.06(s), 1432.94 (m), 1407.59(m), 1300.44(w), 1187.01(w), 1134.73(w), 1058.93(w), 946.76 (w), 762.78 (m), 743.99(s), 651.79 (w).

2.5. *Synthesis of $[Cu_3(p\text{-}3\text{-}bmb)_2Cl_4{\cdot}(CH_3OH)_2]_n$ (4)*

$CuCl_2{\cdot}2H_2O$ (0.0034 g, 0.02 mM), p-3-bmb (0.0065 g, 0.02 mM), chloroform (1 mL), and methanol (1 mL) were placed in a tightly closed glass reactor (10 mL), which was heated at 80 °C for three days and then cooled to room temperature at 5 °C h^{-1}. Dark green crystals of **4** were obtained. Yield: 47% (based on Cu). Elemental analysis (%) Calcd for $C_{40}H_{36}Cl_4Cu_3N_{12}O_2$: C, 45.79%; H, 3.46%; N, 16.02%. Found: C, 45.50%; H, 3.44%; N, 16.18%. IR(KBr/pellet, cm^{-1}): 3439.12(s), 3007.29(w), 1613.76(m), 1455.29(m), 1420.79 (s), 1351.05(w), 1335.57(w), 1192.63(s), 1156.97(m), 1109.25(w), 1058.02(w), 939.50(w), 766.03(s), 752.14(w).

2.6. *Crystal structure determination*

Single crystals suitable for X-ray determination were selected and mounted on a glass fiber. The data for **1** and **3** were recorded on a Gemini E at room temperature with graphite monochromated Mo-Kα radiation ($\lambda = 0.71073$ Å) for **1** and Cu-$K\alpha$ ($\lambda = 1.54184$ Å) for **3**. **2** and **4** were recorded on a SuperNova with graphite monochromated Mo-Kα radiation ($\lambda = 0.71073$ Å) at 100 K. The structures were handled by direct methods and expanded with Fourier techniques. Calculations of **1** and **3** were conducted with SHELXL-97 crystallographic program, whereas **2** and **4** were conducted with the OLEX2 crystallographic program [15]. All non-hydrogen atoms were refined with anisotropic thermal parameters. The final cycle of full-matrix least-squares refinement was based on observed reflections and variable parameters. Table 1 gives the crystallographic crystal data and structure processing parameters of the four complexes, and selected bond lengths and angles are listed in table 2.

2.7. *Cell culture*

SGC7901, EC109, SMMC7721, and HT29 are human gastric, esophagus, liver, and colon carcinoma cell lines, respectively. Cell lines were routinely maintained in the logarithmic phase at 37 °C in a highly humidified atmosphere of 95% air with 5% carbon dioxide using the RPMI1640 medium supplemented with 10% (v/v) heat inactive fetal bovine serum.

2.8. In vitro *antitumor assay*

Copper and zinc complexes were dissolved in DMSO (cell culture reagent) just before the experiment, and complex solution was added to the growth medium containing cells with a final solvent concentration of 3‰, which has hardly discernible effect on cell killing [16].

The growth inhibitory effect of **1–4** on human tumor cell lines was evaluated by MTT (MTT = 3-(4,5-dimethylthiazol-2-yl)-2,5-diphenyltetrazolium bromide) assay, in which MTT is decomposed by living cells to produce DMSO soluble formazan that could be detected through colorimetric analysis. Briefly, cells were seeded in 96-well microplates in growth medium (100 μL) and then incubated at 37 °C in a highly humidified atmosphere with 5% CO_2. Amounts of cells range from 3×10^3 to 8×10^3 cells/well, and the number depends on the growth characteristics of different cell lines. The medium was eliminated and replaced with a fresh one (200 μL) containing the complexes at the appropriate concentration after 24 h. Three test timescales (24, 48, 72 h) were established for each treatment. After the time, 20 μL of MTT solution (5 mg/mL) was added to each well and further incubated for 4 h at 37 °C. Then, the medium with MTT was discarded, and 150 μL of DMSO was added to each well to dissolve the formazan crystals. The absorbance was measured at test wavelength of 492 nm using a microplate reader. Each experiment was

Table 1. Crystal data and structure refinements for **1–4**.

Complex	**1**	**2**	**3**	**4**
Formula	$Cu_2C_{38}H_{28}Cl_4N_{12}$	$C_{38}H_{28}N_{12}Br_4Cu_2$	$Zn_2C_{38}H_{28}Cl_4N_{122}$	$C_{40}H_{36}Cl_4Cu_3N_{12}O_2$
Formula weight	921.60	1099.44	925.26	1049.23
Temperature (K)	293(2)	100(10)	291(2)	100(2)
λ (Mo Cu/Kα) Å	0.71073	0.71073	1.54184	0.71073
Crystal system	Monoclinic	Monoclinic	Triclinic	Triclinic
Space group	$P2_1/c$	$P2_1/c$	P-1	P-1
a (Å)	9.7287(5)	9.7525(16)	7.2824(4)	9.2155(8)
b (Å)	13.2327(10)	13.3114(2)	9.3963(7)	9.9581(8)
c (Å)	14.8185(9)	14.9482(2)	14.2591(9)	12.2028(10)
α (°)	90.00	90.00	92.337(6)	97.482(7)
β (°)	99.443(6)	99.10(16)	91.315(5)	110.398(8)
γ (°)	90.00	90.00	96.975(5)	94.259(7)
V (Å^3)	1881.8(2)	1916.14(5)	967.32(11)	1032.02(15)
Z	2	2	1	1
F(0 0 0)	932	1076.0	468	531
θ range for data collection (°)	3.07–26.31	3.06–26.34	3.10–66.96	2.95–26.37
Final R_1[a], wR_2[b]	0.0411, 0.0815	0.0345, 0.0902	0.0356, 0.0915	0.0368, 0.0874
Goodness-of-fit on F^2	1.047	0.984	1.033	1.041

[a]$R_1 = ||F_o| - |F_c||/|F_o|$. [b]w$R_2 = [w(|F_o^2| - |F_c^2|)^2/w|F_o^2|^2]^{1/2}$. $w = 1/[\sigma^2(F_o)^2 + 0.0297P^2 + 27.5680P]$, where $P = (F_o^2 + 2F_c^2)/3$.

Table 2. Selected bond distances (Å) and angles (°) for **1–4**.

Complex **1**			
Cu(1)–N(1)	2.047(2)	Cu(1)–N(6)#1	2.408(2)
Cu(1)–N(3)	2.063(3)	Cu(1)–Cl(1)	2.2688(9)
Cu(1)–Cl(2)	2.2427(9)	Cl(2)–Cu(1)–Cl(1)	93.03(4)
Cl(1)–Cu(1)–N(6)#1	104.14(7)	Cl(2)–Cu(1)–N(6)#1	98.46(7)
Cl(2)–Cu(1)–N(1)	95.63(7)	N(1)–Cu(1)–N(6)#1	94.67(9)
Cl(1)–Cu(1)–N(1)	157.88(7)	N(1)–Cu(1)–N(3)	79.49(10)
Complex **2**			
Cu(1)–N(1)	2.062(3)	Cu(1)–N(2)	2.057(3)
Cu(1)–N(6)#1	2.371(3)	Cu(1)–Br(1)	2.3695(6)
Cu(1)–Br(2)	2.4265(6)	N(1)–Cu(1)–N(2)	79.94(12)
N(1)–Cu(1)–N(6)#1	79.08(12)	N(2)–Cu(1)–N(6)#1	97.10(12)
N(1)–Cu(1)–Br(1)	174.51(9)	N(2)–Cu(1)–Br(2)	156.47(9)
N(6)#1–Cu(1)–Br(1)	97.96(8)	N(1)–Cu(1)–Br(2)	93.42(9)
Complex **3**			
Zn(1)–Cl(1)	2.2215(8)	Zn(1)–Cl(2)	2.2281(8)
Zn(1)–N(1)	2.075(2)	Zn(1)–N(3)#1	2.047(2)
Cl(1)–Zn(1)–Cl(2)	115.54(3)	Cl(1)–Zn(1)–N(1)	111.73(7)
Cl(2)–Zn(1)–N(1)	107.49(6)	Cl(1)–Zn(1)–N(3)#1	108.97(7)
Cl(2)–Zn(1)–N(3)#1	109.27(7)	N(1)–Zn(1)–N(3)#1	103.09(8)
Complex **4**			
Cu(1)–N(1)	1.998(2)	Cu(1)–N(1)#1	1.998(2)
Cu(1)–Cl(2)	2.3520(7)	Cu(1)–Cl(2)#1	2.3520(7)
Cu(2)–N(2)	1.889(2)	Cu(2)–Cl(1)#1	2.1201(8)
N(1)–Cu(1)–N(1)#1	180.0(1)	N(1)–Cu(1)–Cl(2)	90.21(7)
N(1)#1–Cu(1)–Cl(2)	89.79(7)	N(1)#1–Cu(1)–Cl(2)#1	90.21(7)
N(2)–Cu(2)–Cl(1)	165.67(7)	Cl(2)–Cu(1)–Cl(2)#1	180.0

Symmetry transformations used to generate equivalent atoms: #1 $1-x$, $2-y$, $2-z$ for **1**; #1 $2-x$, $1-y$, $2-z$ for **2**; #1 $-x$, $2-y$, $2-z$ for **3**; #1 $1-x$, $1-y$, $1-z$ for **4**.

repeated three times to get the mean values. The % cell inhibition was determined as follows: % cell inhibition = $(1 - \mathrm{Abs}_{\text{treated cells}}/\mathrm{Abs}_{\text{control cells}}) \times 100\%$. Results were expressed as IC_{50}, which is the concentration of complexes required to induce 50% inhibition of cell growth. They were calculated on the basis of cell inhibition with modified Karber's method.

3. Results and discussion

3.1. *Crystal structures of 1 and 2*

X-ray diffraction analyses indicate that **1** and **2** have similar binuclear structures based on the same ligand and crystallize in monoclinic space group $P2_1/c$. Instead of acetate from $Cu(Ac)_2{\cdot}H_2O$, two Cl^- are contributed to the coordination in **1** from decomposition of chloroform in the synthesis. As shown in figure 1, the Cu(II) in **1** is five-coordinate in a distorted trigonal bipyramidal coordination geometry, completed by two Cl^- (Cl1, Cl2) and three nitrogens (N1, N3 from one p-2-bmb molecule and N6′ from the other one). Cl1 and N1 occupy apical positions with Cl(1)–Cu(1)–N(1) angle of 157.88(7)°, and N3, N6′, and Cl2 are coplanar. The Cu–N distances are Ë…2.047–2.408 Å and Cu–Cl bond lengths are 2.269 and 2.243 Å for Cu1–Cl1and Cu1–Cl2, respectively.

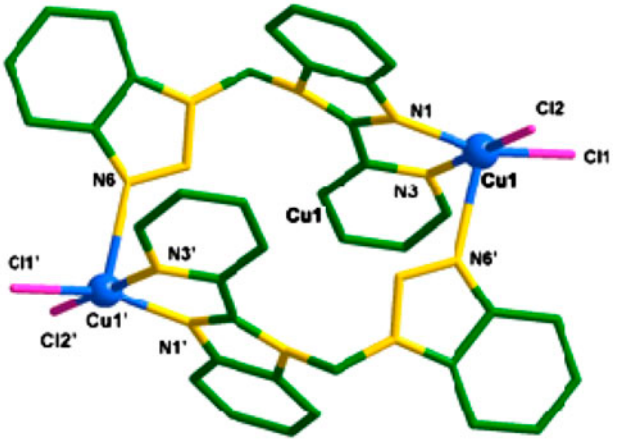

Figure 1. The binuclear cycle motif of **1** (all hydrogens are omitted for clarity).

The $Cu(Ac)_2{\cdot}H_2O$ salt was replaced by $CuBr_2$ giving binuclear **2**, which is similar to **1**. For **2**, the Cu(II) also is five-coordinate with distorted trigonal bipyramidal coordination geometry. The asymmetric unit (figure 2) consists of one Cu(II) center, two bromides, and one ligand. Each Cu(II) is coordinated by two Br^- (Cu–Br1 = 2.3695 Å, Cu–Br2 = 2.4265 Å) and three nitrogens from two p-2-bmb molecules (N1, N2, N6′ with Cu–N vary from 2.057 to 2.371 Å).

In **1** and **2**, there are $\pi\ldots\pi$ interactions between two parallel adjacent imidazole rings and adjacent imidazole ring to benzene ring (3.8577 Å and 0°, 3.5635 Å and 0.531° for **1**, 3.847 Å and 0°, 3.587 Å and 0.925° for **2**), and some carbons and halides are alternatively linked by hydrogen bonds. Thus, **1** and **2** form 3D supramolecular frameworks (figures 3 and Supplementary material.doc).

Due to different anionic radii of Cl^- and Br^-, the coordination geometries of Cu(II) centers are slightly different and hydrogen bond lengths in **2** are slightly longer than those in **1** (3.573 Å for C13…Cl1′, 3.631 Å for C11…Cl2′, 3.645 Å for C15…Cl2′, 3.748 Å for C13…Cl2′ in **1** and 3.625 Å for C11…Br1′, 3.677 Å for C13(H13B)…Br2′, 3.701 Å for C15…Br1′, 3.818 Å for C13(H13A)…Br1′ in **2**).

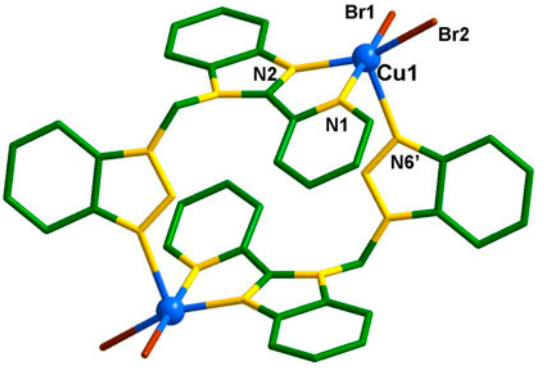

Figure 2. The binuclear cycle motif of **2** (all hydrogens are omitted for clarity).

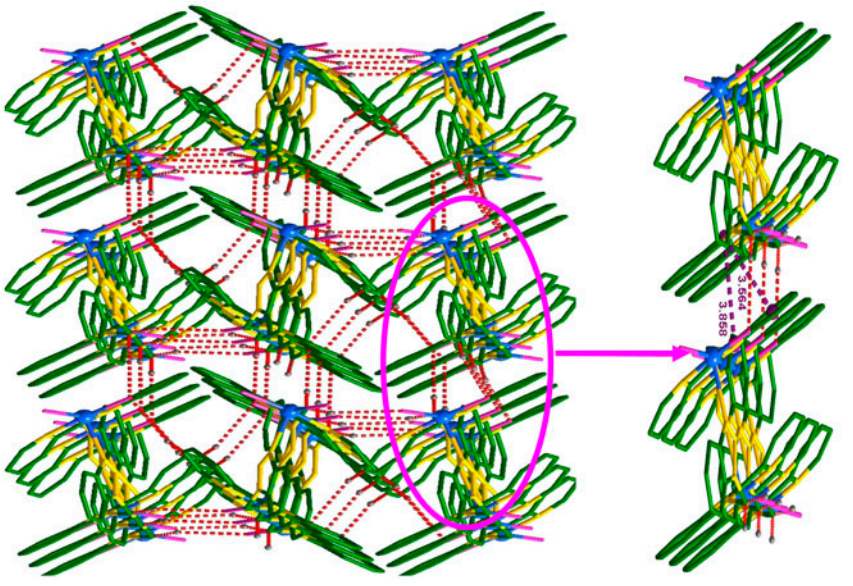

Figure 3. View of 3D supramolecular structure of **1** stabilized by hydrogen–bonding and $\pi\cdots\pi$ interactions.

3.2. *Crystal structures of 3 and 4*

Complex **3** based on p-3-bmb is binuclear, crystallizing in the triclinic space group P-1. As shown in figure 4, each Zn(II) in **3** is four-coordinate by two p-3-bmbs and two chlorides in a distorted tetrahedral configuration. The tetrahedron is defined by Cl1, Cl2, N1, and N3′, with Zn–Cl distances of 2.2215 and 2.2281 Å, and Zn1–N1 and Zn1–N3′ bond lengths of 2.075 and 2.047 Å, respectively. P-3-bmb in this structure is bidentate; the benzotriazole does not participate in coordination. There exist two $\pi\ldots\pi$ interactions in parallel adjacent triazole rings from p-3-bmbs with centroid separations of 3.8099 and 3.7438 Å. From $\pi\ldots\pi$ interactions and hydrogen bonds (3.365 Å for C4…N5′, 3.610 Å for C13…Cl2′), the binuclear structures are extended into a 3D supramolecular architecture (figure 5).

The replacement of $ZnCl_2$ in **3** by $CuCl_2$ gives an entirely different motif for **4**. **4** also crystallizes in the triclinic space group P-1 and benzotriazole does not coordinate. In contrast to **3**, an infinite chain structure is present due to bridging chloride. The p-3-bmb with uniform coordination fashion gives distinct structures for **3** and **4**. The geometrical and electronic properties of the metal centers may be the primary contributing factor.

As depicted in figure 6, the asymmetric unit of **4** consists of one and a half independent copper centers with different coordination number and different valence. Cu1 lies in a distorted octahedral geometry, in which the equatorial positions are furnished by four Cl^- (Cl1, Cl2, Cl1′, and Cl2′), and the axial sites are occupied by N1 and N1b from two p-3-bmb molecules. Cu2 is in a triangular coordination, completed by two Cl^- and N2 from bridging p-3-bmb. Cu1 and Cu2 are bridged by four Cl^- with Cu1⋯Cu2 separation of 3.560 Å (Cu1⋯Cu2 = Cu1…Cu2′) in trimetallic units (figure 6). Such trimetallic moieties are further connected by p-3-bmb connectors to generate a chain motif (figure S2). Based on $\pi\ldots\pi$ stacking interactions between adjacent imidazole to benzene rings with the

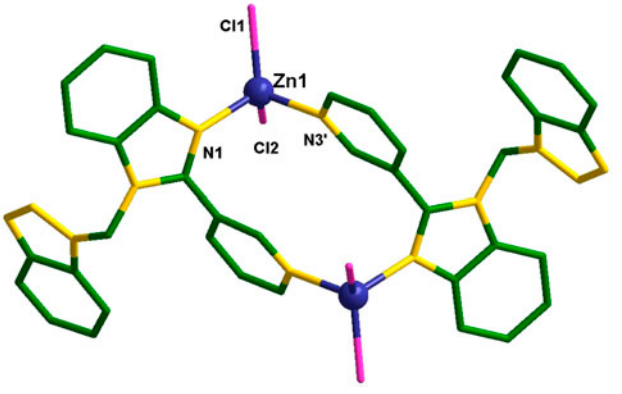

Figure 4. The binuclear cycle motif of **3** (all hydrogens are omitted for clarity).

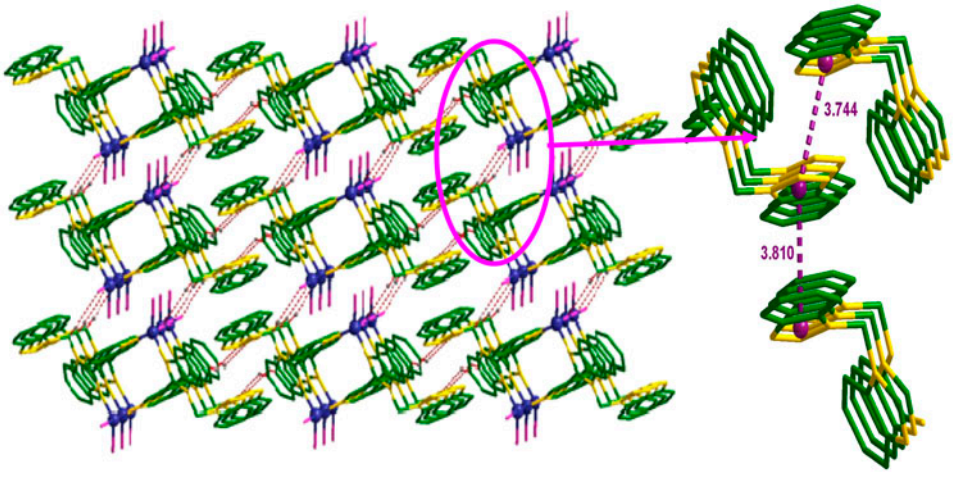

Figure 5. View of 3D supramolecular structure of **3** stabilized by hydrogen–bonding and $\pi\cdots\pi$ interactions.

centroid–centroid distance of 3.583 Å and dihedral angle of 2.281°, and hydrogen bonds (2.846 Å for O1…N6′, 3.172 for C3…O1, 3.681 Å for C13…Cl2′), such chains are assembled into a 3D supramolecular network (figure S3).

3.3. *Thermogravimetric analysis of 4*

To characterize **4** (with solvent molecules) in terms of thermal stability, the thermal behavior was investigated by TGA from 30 to 790 °C at a heating rate of 10 °C/min under air. Complex **4** is air-stable and retains crystalline integrity at room temperature. As shown in figure S4, the first weight loss of **4** takes place between 30 °C and 251 °C, corresponding to release of CH_3OH (calcd: 6.11%, found: 5.25%). After that, **4** decomposes completely by 658 °C. The remaining residue is presumed to be CuO (calcd: 15.16%; found: 14.25%). The DSC spectrum exhibits an exothermic peak near 643 °C, which may indicate that **4** completely decomposed.

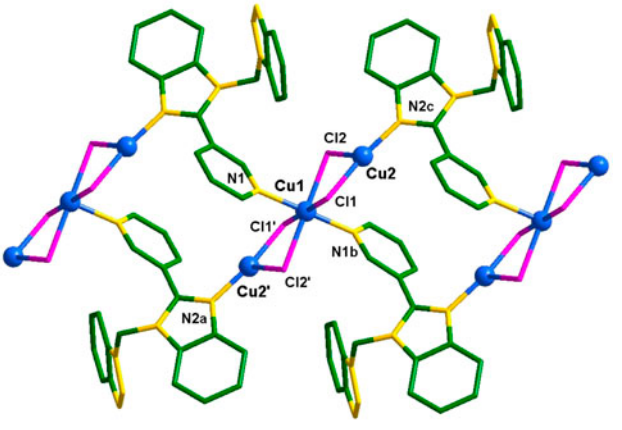

Figure 6. The coordination environment of copper in **4** (all hydrogens and solvent molecules are omitted for clarity).

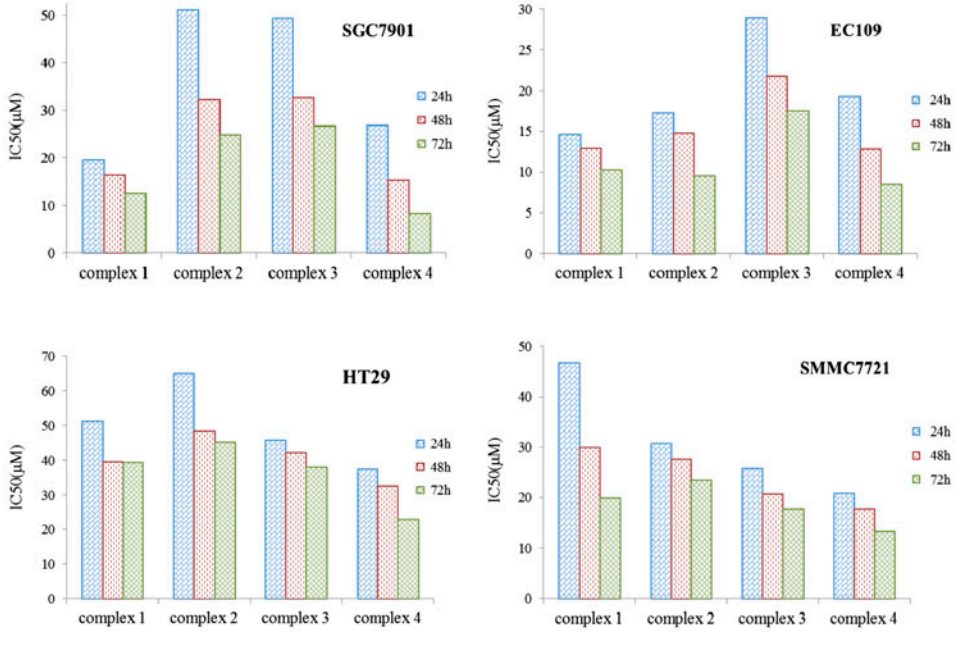

Figure 7. The IC_{50} values of complexes against SGC7901, EC109, HT29, SMMC7721 cells.

3.4. In vitro *antitumor activity of complexes*

The cytotoxicities of **1–4** were assessed with the standard MTT assays using human tumor cell lines. All the complexes dissolved in DMSO with certain concentration and a blank sample with the same volume of DMSO was provided as a control. As shown in figure 7, the IC_{50} values reveal that these complexes inhibit the four human alimentary system tumor cell lines, especially EC109. Except for HT29, the inhibition is time dependent. Complex **4** expresses more potent inhibition on SGC7901, EC109, and SMMC7721 with

IC_{50} values (μM) of 8.22, 8.49, 13.37 for 72 h, respectively. **1** is a more potent inhibitor of SGC7901 and EC109 cells, and **2** exhibits high cytotoxicity against EC109 and SMMC7721 cells, whereas **3** shows antiproliferative activity to SMMC7721 cells. By comparison, cisplatin, as a clinical anti-cancer drug with strong cytotoxic activity to most tumor cell lines *in vitro*, was also investigated against the four cell lines under the same conditions. The IC_{50} values of cisplatin (μM) in the cells of SGC7901, EC109, and HT29 were 10.92, 10.75, 7.53 for 72 h, respectively; cisplatin has almost no effect on the viability of the SMMC-7721 cells.

Although **1**, **2,** and **3** with different compositions display binuclear motifs, p-2-bmb and p-3-bmb adopt different coordination geometries. By comparison, **4** is a 1D chain structure based on trimetallic fundamental unit, and the arrangement of ligands is different from **1–3**. The benzotriazole of the complexes may affect cell proliferation. These results extend the benzotriazole and benzimidazole-based structure–activity relationships, indicating synergic combination of the ligand and the metal centers play a crucial role on the cytotoxic effects. Small alterations of orientation and structure may lead to considerable changes in the interaction modes and selective transport across the cancer cell membrane under physiological conditions.

4. Conclusions

Four new complexes based on flexible p-2-bmb or p-3-bmb have been synthesized under solvothermal reaction and characterized. The $\pi\cdots\pi$ interactions and hydrogen bonds play significant roles in structures and stabilization of **1–4**. The *in vitro* antitumor activities of the complexes on human tumor cell lines (SGC7901, EC109, SMMC7721, HT29) were evaluated by MTT assay. Based on the synergetic effects of metal centers and aromatic bridging connectors, the benzotriazole and benzimidazole-based complexes may have interactions with site-specific bases of tumor cell lines to account for the cytotoxic activities.

Supplementary data

Crystallographic data for the structural analysis have been deposited with the Cambridge Crystallographic Data Center, CCDC reference numbers 890348–890351. These data can be obtained free of charge via www.ccdc.cam.ac.uk/conts/retrieving.htm (or from the Cambridge Crystallographic Data Center, 12 Union Road, Cambridge CB2 1EZ, UK; Fax: +44 1223 336,033).

Acknowledgments

We gratefully acknowledge the financial support by the Talent Supporting Plan of He'nan Scientific and Technological Innovation (No. 2010HASTIT016) and the He'nan key science and technology research (No. 102102310079 and 112102310084).

References

[1] (a) M.A. Braverman, P.J. Szymanski, R.M. Supkowski, R.L. LaDuca. *Inorg. Chim. Acta*, **360**, 3684 (2009); (b) E.C. Spencer, R.J. Angel, N.L. Ross, B.E. Hanson, J.A.K. Howard. *J. Am. Chem. Soc*., **131**, 4022 (2009); (c) Z.R. Pan, J. Xu, H.G. Zheng, K.X. Huang, Y.Z. Li, Z.J. Guo, S.R. Batten. *Inorg. Chem*., **48**, 5772 (2009).

[2] (a) Z. Chang, D.S. Zhang, T.L. Hu, X.H. Bu. *Cryst. Growth Des*., **11**, 2050 (2011); (b) W. Liu, X. Chen, Q. Ye, Y. Xu, C. Xie, M. Xie, Q. Chang, L. Lou. *Inorg. Chem*., **50**, 5324 (2011); (c) A. Banisafar, D.P. Martin, J.S. Lucas, R.L. LaDuca. *Cryst. Growth Des*., **11**, 1651 (2011); (d) X. Feng, J.G. Wang, B. Liu, L.Y. Wang, J.S. Zhao, S. Ng. *Cryst. Growth Des*., **12**, 927 (2012).
[3] Y. Wang, X. Wang, J. Wang, Y. Zhao, W. He, Z. Guo. *Inorg. Chem.*, **50**, 12661 (2011).
[4] P. Mura, F. Piccioli, C. Gabbiani, M. Camalli, L. Messori. *Inorg. Chem.*, **44**, 4897 (2005).
[5] (a) F. Caruso, C. Pettinari, F. Marchetti, P. Natanti, C. Phillips, J. Tanski, M. Rossi. *Inorg. Chem*., **46**, 7553 (2007); (b) M.S. Balakrishna, D. Suresh, A. Rai, J.T. Mague, D. Panda. *Inorg. Chem*., **49**, 8790 (2010); (c) J.Y. Xu, Y. Zeng, Q. Ran, Z. Wei, Y. Bi, Q.H. He, Q.J. Wang, S. Hu, J. Zhang, M.Y. Tang, W.Y. Hua, X.M. Wu. *Bioorg. Med. Chem. Lett*., **17**, 2921 (2007).
[6] (a) Z. Ates-Alagoz, S. Yildiz, E. Buyukbingol. *Chemotherapy*, **53**, 110 (2007); (b) H.L. Wu, K. Li, T. Sun, F. Kou, F. Jia, J.K. Yuan, B. Liu, B.L. Qi. *Transition Met. Chem*., **36**, 21 (2011); (c) R. Balamurugan, M. Palaniandavar. *Inorg. Chem*., **40**, 2246 (2001).
[7] S. Padhye, Z. Afrasiabi, E. Sinn, J. Fok, K. Mehta, N. Rath. *Inorg. Chem.*, **44**, 1154 (2005).
[8] (a) R. Starosta, K. Stokowa, M. Florek, J. Krol, A. Chwiłkowska, J. Kulbacka, J. Saczko, J. Skała, M. Jeowska-Bojczuk. *J. Inorg. Biochem*., **105**, 1102 (2011); (b) S. Anbu, S. Kamalraj, B. Varghese, J. Muthumary, M. Kandaswamy. *Inorg. Chem*., **51**, 5580 (2012); (c) H. Kozlowski, A. Janicka-Klos, J. Brasun, E. Gaggelli; D. Valensin, G. Valensin. *Coord. Chem. Rev*., **253**, 2665 (2009).
[9] X. Qiao, Z.Y. Ma, C.Z. Xie, F. Xue, Y.W. Zhang, J.Y. Xu, Z.Y. Qiang, J.S. Lou, G.J. Chen, S.P. Yan. *J. Inorg. Biochem.*, **105**, 728 (2011).
[10] S. Gama, F. Mendes, F. Marques, I.C. Santos, M.F. Carvalho, I. Correia, J.C. Pessoa, I. Santos, A. Paulo. *J. Inorg. Biochem.*, **105**, 637 (2011).
[11] Q.Y. Chen, J. Huang, W.J. Guo, J. Gao. *Spectrochim. Acta, Part A*, **72**, 648 (2009).
[12] D. Kovala-Demertzi, A. Alexandratos, A. Papageorgiou, P.N. Yadav, P. Dalezis, M.A. Demertzis. *Polyhedron*, **27**, 2731 (2008).
[13] A.W. Addison, P.J. Burke. *J. Heterocycl. Chem.*, **18**, 803 (1981).
[14] A. Yoshimura, K. Nozaki, N. Ikeda, T. Ohno. *Bull. Chem. Soc. Jpn.*, **69**, 2791 (1996).
[15] (a) G.M. Sheldrick, *SHELXTL-97*, *Program for Crystal Structure Refinement*, University of Göttingen, Germany (1997); (b) G.M. Sheldrick, *SHELXS-97*, *Program for Crystal Structure Solution*, University of Göttingen, Germany (1997); (c) G.M. Sheldrick. *Acta Crystallogr., Sect. A*, **64**, 112 (2008); (d) O.V. Dolomanov, L.J. Bourhis, R.J. Gildea, J.A. K. Howard, H. Puschmann. *J. Appl. Crystallogr.*, **42**, 339 (2009).
[16] M. Porchia, F. Benetollo, F. Refosco, F. Tisato, C. Marzano, V. Gandin. *J. Inorg. Biochem.*, **103**, 1644 (2009).